Manuscript: Fennoscandian tree-ring anatomy shows modern climate warmer than Medieval

Jesper Björklund [1, 2, †], Kristina Seftigen [1, 3], Markus Stoffel [4, 5, 6], Marina V. Fonti [1, 2], Sven Kottlow [1], David C. Frank [7], Jan Esper [8, 9], Patrick Fonti [1, 2], Hugues Goosse [10], Håkan Grudd [11], Björn E. Gunnarson [12, 13], Daniel Nievergelt [1, 2], Elena Pellizzari [14], Marco Carrer* [14] & Georg von Arx* [1, 2]

Affiliations

[1] Swiss Federal Institute for Forest Snow and Landscape Research WSL, Birmensdorf, Switzerland
[2] Oeschger Centre for Climate Change Research, University of Bern, Switzerland
[3] Regional Climate Group, Department of Earth Sciences, University of Gothenburg, Sweden
[4] Climatic Change and Climate Impacts, Institute for Environmental Sciences, University of Geneva, Switzerland.
[5] Dendrolab.ch, Department of Earth Sciences, University of Geneva, Switzerland.
[6] Department F.-A. Forel for Environmental and Aquatic Sciences, University of Geneva, Switzerland.
[7] Laboratory of Tree-Ring Research, University of Arizona, USA
[8] Department of Geography, Johannes Gutenberg University, Mainz, Germany
[9] Global Change Research Institute of the Czech Academy of Sciences (CzechGlobe), Brno, Czech Republic
[10] Earth and Life Institute, Université Catholique de Louvain (UCLouvain), Louvain-la-Neuve, Belgium
[11] Swedish Polar Research Secretariat, Abisko Scientific Research Station, Sweden.
[12] Department of Physical Geography, Stockholm University, Sweden
[13] Bolin Centre for Climate Research, Stockholm University, Sweden
[14] Department of Land Environment Agriculture and Forestry (TeSAF), University of Padova, Legnaro, Italy

Corresponding author: Jesper Björklund
Email: jesper.bjoerklund@wsl.ch
[†]Address: Swiss Federal Institute for Forest Snow and Landscape Research WSL, Zuercherstrasse 111, 8903 Birmensdorf, Switzerland

*These authors contributed equally to this work

This document is the accepted manuscript version of the following article:
Björklund, J., Seftigen, K., Stoffel, M., Fonti, M. V., Kottlow, S., Frank, D. C., … von Arx, G. (2023). Fennoscandian tree-ring anatomy shows a warmer modern than medieval climate. Nature, 620(7972), 97-103. https://doi.org/10.1038/s41586-023-06176-4

Abstract

Current global warming is unprecedented over at least the Common Era according to Earth system models and various climate proxy sources [1]. Yet, tree-ring proxies often portray the Medieval Climate Anomaly (MCA; 950-1250 CE) with temperatures similar to, or exceeding, those recorded in the past century [2,3], thereby contrasting markedly with simulation experiments at regional scales [4]. This not only call into question the reliability of models and proxies, but also contributes to uncertainty in future climate projections [5]. Here we show that Fennoscandian climate is substantially warmer today than during the Medieval. This highlights the dominant role of anthropogenic forcing on climate warming even at the regional scale, thereby reconciling inconsistencies between reconstructions and model simulations. The new evidence is based on an annually resolved 1170-year-long tree-ring record that relies exclusively on tracheid anatomical measurements from *Pinus sylvestris* trees representing warm season instrumental temperature variability at unprecedented fidelity. We therefore call for the construction of more such millennia-long records to further improve our understanding and reduce uncertainties around historical and future climate change at inter-regional and eventually global scales.

Main Manuscript

Over the past decades, considerable effort and debate have been devoted to how putative climate episodes, such as the Medieval Climate Anomaly (MCA; 950-1250 CE) or the Little Ice Age (LIA; 1450-1850 CE) are characterized and relate to the Current Warm Period (CWP) [6-8]. Although the view that CWP is globally warmer than any other period over the Common Era is firmly consolidated [1], large uncertainties persist in models and proxies at regional scales, particularly prior to 1400 CE [3,8-10]. In Europe, the Medieval warming is actually found equal to, or occasionally warmer than 20th century temperatures [3], fueling narratives such as being critical for Norse settlements in Greenland in 985 CE [11]. However, an exceptionally warm MCA is difficult to reconcile with forced climate model simulations [4], thus suggesting larger and more persistent unforced climate variability than the models presently produce. Reducing uncertainties, particularly during the MCA and the Medieval Quiet Period (MQP; 725-1025 CE) [12], is therefore critically needed to further evaluate the sensitivity and internal variability of the climate system [13], not least with the perspective of rendering future projections more robust [5]. The focus on MQP and MCA is a particularly important benchmark for the amplitude of *natural* climate variability

due to the limited volcanic, and relatively unperturbed solar forcing [12] to compare with the *anthropogenically* forced CWP.

Tree-ring data are central to the majority of empirical studies characterizing temperature change of the Common Era [14], and are therefore especially subjected to scientific critiques on their ability to capture key characteristics of historical climate variations [15-21]. Debates are particularly vigorous around the two most prominent proxy sources – tree-ring width and maximum latewood density (MXD) – to intrinsically reflect climate change over millennia [15,16,22], to track the full amplitude of climate extremes [21,23-25], or for spectrally biased transformations from climate [17-19,24,26]. Recent progress in retrieving information from tree rings [27,28] have thus inquired whether some of these uncertainties could be alleviated by directly analyzing the dimensions of the wood cells (Fig. 1). This quantitative wood anatomical (QWA) approach offers unparalleled measurement precision [29], and often substantial gains in climate fidelity [30-33] when used in tree-rings. Yet, no tree-ring anatomy record has hitherto been produced to assess both the natural and anthropogenic range of climate variability over longer time periods and with sufficient robustness.

Here we develop a novel QWA-based 1170-year-long reconstruction of warm season temperature (May-August) using 188 living and dead *Pinus sylvestris* (Scots pine) trees from Fennoscandia (A-FEN). This region hosts a disproportionate share of the millennial length tree-ring datasets around the arctic circle and is thus exceedingly influential in shaping our view of past climate in this sensitive area *and* elsewhere. Although these records constitute some of the most skillful examples of Common Era temperature reconstructions [20], climate variability and change during the MCA, LIA and CWP has repeatedly been revised and questioned [2,16,34-37]. We therefore subject the A-FEN to an array of tests, including comparisons with relevant reconstructions [1,2,9,10,37-39] and climate model simulations within the Coupled and Paleo Model Intercomparison Projects Phases (CMIP5/PMIP3) [40-52]. Relying on the A-FEN, we put the recent warming into a robust long-term context providing critical insights into climate dynamics in the region which in turn will increase confidence in model projections [52].

Elevated proxy calibration skill

The tree-ring anatomy data in A-FEN was randomly resampled into an ensemble of 100 datasets (each member with a maximum replication of 15 trees/year), explaining 71-79% of the variance in regional May-August temperatures (Fig. 2a). The total A-FEN replication never falls below 20 trees/year, and the average pairwise correlation between trees (Rbar [53]) is high, thus suggesting stable reconstruction skill during 850-1849 CE (Fig. 2b). The A-FEN tightly tracks the increasing temperature trend, captures c. 80% of both cold *and* warm extremes (Extended Data Fig. 1), and exhibits a similar first-order autocorrelation as the May-August temperatures (Extended Data Fig. 2). Results remain virtually the same regardless if idiosyncratic signal processing (known as standardization/detrending in the tree-ring literature [54]) is used (Extended Data Fig. 3). This means that the A-FEN is essentially free of artificial climate-signal distortion that can occur when attempting to remove non-climate variability [15].

Although the climatic imprint in A-FEN is similar to the MXD-based corresponding reconstruction [9] (hereafter X-FEN), A-FEN is significantly stronger (Fig. 2a), and consistently performs better across inter-annual to decadal timescales (Extended Data Fig. 2). A-FEN is potentially less susceptible to fading reconstruction quality than X-FEN. This is because X-FEN Rbar and replication calculated over the calibration period (1850-2019) substantially exceeds corresponding statistics for the reconstruction period (850-1849) (Fig. 2b). Moreover, A-FEN is not appreciably biased by extremely narrow rings (Extended Data Fig. 4). For instance, widespread pine tree canopy damage took place across Fennoscandia in the winter/spring of 1902/1903 [55], leading to reduced photosynthetic capacity and persistent reductions in wood cell divisions [56], and thus ring widths [57]. This episode is significant because it represents a temporary collapse of climate as dominant control over ring width. Nevertheless, A-FEN continues to track May-August temperatures revealing that the collapse only affects cell *divisions* (ring width) but not cell *dimensions*. In contrast, X-FEN systematically underestimates summer temperatures during this period (Fig. 2a), suggesting that these X-ray measurements are affected by extremely narrow rings, and thus contains more biological noise. The X-FEN is also less independent of narrow rings on *average* (Extended Data Fig. 4c and 5), suggesting latent measurement artifacts during the pre-instrumental era. In summary, the A-FEN provides a more robust and skillful reconstruction of warm season temperatures than X-FEN, and the linear reconstruction model is well verified in three split-sample calibration/verification periods (Extended Data Tab. 1).

Revised long-term climate context

The A-FEN displays a gently negative long-term trend between 850 and 1850, followed by a sharp temperature rise (Fig. 2). The peak medieval warmth in A-FEN and X-FEN occurs around 850-1100 (hereafter MCA*) when the A-FEN exhibits modest centennial-scale variability, consistent with a lack of volcanic, and stable solar forcing [12]. The onset of the LIA is preceded by a relatively warm period around 1400, interrupted by a rapid cooling, possibly driven by the still unidentified volcanism around 1453 [58]. Temperatures also briefly warm up in the late 18th century. This temperature evolution is stable regardless of which 15 trees/year are resampled from A-FEN (Extended Data Fig. 6), and it is remarkably similar to reconstructed Northern Hemisphere summer temperatures and even global annual temperatures (Fig. 2c). The multi-decadal fluctuations of A-FEN are similar to those of X-FEN, but X-FEN most notably portrays MCA* as exceptionally warm, and CWP only with above average temperatures (Fig. 2c). X-FEN is consistently included in the hemispheric and global reconstructions (Fig. 2c), it will therefore also elevate medieval and suppress current temperatures in these products. However, when several millennium-length Fennoscandian MXD datasets commonly used in larger-scale reconstructions [1,6,9,10,14,39,59-63] are explored, the data show a wide range of medieval temperature estimates (Extended Data, Fig. 7a), underscoring the large uncertainty during this period. The inclusion of the new A-FEN reconstruction would thus likely reduce this uncertainty and provide a valuable new benchmark for a modestly warm Medieval and a substantially warmer present.

Proxy-model agreement

The spectral properties, and first-order autocorrelation of A-FEN are very similar to those of the model ensemble (Extended Data Fig. 8). It is noteworthy that A-FEN and most model ensemble outputs agree, particularly in the frequency of warm extremes with a significant overrepresentation of the 100 warmest summers in the recent century (Fig. 3a). The coldest years in the A-FEN and X-FEN are often associated with volcanic activity, namely the unidentified eruption 1453, Eldgjá 939, Huaynaputina 1600, and Parker 1640 CE. By contrast, two of the largest volcanic eruptions of the past millennium, Samalas 1257 and Tambora 1815, do not appear to have caused detectable cooling in Fennoscandia (Extended Data Fig. 9). The climate models used in this study produce comparably distinct cooling patterns on average, yet with important differences for specific events.

Model simulations of regional summer temperatures reveal overarching patterns that strongly resemble those of the new A-FEN reconstruction, while again highlighting an MCA* and CWP mismatch with X-FEN (Fig 3b). At regional scales, such as in Fennoscandia, substantial internal climate variability – both implemented in models and imprinted in proxy observations – tends to diverge as these stochastic components are by definition not synchronized [64]. Therefore, it is particularly encouraging that the models and A-FEN agree, in terms of (1) statistical properties of the temperature history (e.g., incidence of warm extremes, spectral characteristics), (2) responses to volcanic and anthropogenic forcing, and (3) the amplitude and warming of the quietly forced climate variability around the medieval period. We also note that A-FEN is consistent with orbitally forced cooling over the past millennium [16], while at the same time characterizing the impact of anthropogenic forcing as much more influential.

Warm Medieval but hotter present

Unlike reconstructions relying on other tree-ring parameters, the A-FEN record realistically tracks the full breadth of recent climate extremes [21,23-25], and appears to provide a spectrally unbiased transformation from climate to proxy record [17-19,24,26], via tree biological process. Although the debate over whether tree-ring proxies reflect climate change over millennial timescales [15,16,22] will continue, we note that this study is the first to identify close agreement between model and proxy records over these time scales. The novel A-FEN reconstruction thus shows that the recent warming in Fennoscandia far exceeds the natural variability of the past millennium, in contrast to what was previously reported [3], and highlights the impact and occurrence of anthropogenic forcing on climate warming even at the regional scale. The difference from X-FEN could therefore not be more consequential. The MCA* reconstructed using X-FEN is in contrast significantly warmer than A-FEN's account for the same period (Fig. 4), which would deemphasize the role of anthropogenic forcing on Fennoscandian climate variability. This large difference is difficult to explain only with technical improvements provided by the QWA approach and is similarly difficult to explain referring to a slightly imperfect sample overlap (Methods) given the homogenous sub-sampling results of A-FEN (Extended Data Fig. 6). However, the empirical evidence and theoretical advantages presented in this study, strongly support the A-FEN representation of past temperature variability and is further strengthened by the compatibility with independent large-scale reconstructions and climate models.

Climate models integrate current knowledge of system physics and are consistent with past climate dynamics at the event scale (e.g., volcanoes) as well as at broader trends (e.g., rise in current temperatures). The completely independent tree-ring anatomy observations instead draw strength from an exceptional fidelity to instrumental climate variations, is theoretically less susceptible to measurement related artifacts, and exhibit a balanced dataset in terms of tree-replication and correlations among trees outside the period of instrumental observations. Since the forced models, as well as A-FEN, are both unable to reproduce an exceptionally warm medieval period [3,4], their alignment thus forms compelling new evidence for a more moderate MCA* than previously estimated [2,3,16,34,35,37,61]. The new-found proxy-model alignment may additionally have benefitted from the reduced biological noise in A-FEN, which is more closely resembling the noise-free structure of model simulations [63].

Provided that revised temperature characterization and proxy capabilities using tree-ring anatomy become standard, (1) the troubling underestimates of temperatures observed in recent years, also known as "divergence" [65], seen in large-scale reconstructions (e.g., [9,10,66]) and hinted in Extended Data Fig. 7, could possibly be mitigated. (2) The uncertainties prior to 1400 CE could likely be reduced and provide a valuable new constraint on quietly forced natural climate variability. In conjunction with model simulations, reconstructions of current and medieval climate using tree-ring anatomy could thus strengthen benchmarks of natural and anthropogenically forced climate variability and importantly benefit climate models and their projections.

References

1 Neukom, R. *et al.* Consistent multi-decadal variability in global temperature reconstructions and simulations over the Common Era. *Nature geoscience* **12**, 643 (2019).

2 Esper, J., Düthorn, E., Krusic, P. J., Timonen, M. & Büntgen, U. Northern European summer temperature variations over the Common Era from integrated tree-ring density records. *Journal of Quaternary Science* **29**, 487-494 (2014).

3 Luterbacher, J. *et al.* European summer temperatures since Roman times. *Environmental research letters* **11**, 024001 (2016).

4 Fernández-Donado, L. *et al.* Large-scale temperature response to external forcing in simulations and reconstructions of the last millennium. *Climate of the Past* **9**, 393-421 (2013).

5 Masson-Delmotte, V. *et al.* Climate change 2021: the physical science basis. *Contribution of working group I to the sixth assessment report of the intergovernmental panel on climate change*, 2 (2021).

6 Neukom, R., Steiger, N., Gómez-Navarro, J. J., Wang, J. & Werner, J. P. No evidence for globally coherent warm and cold periods over the preindustrial Common Era. *Nature* **571**, 550-554 (2019).

7 Frank, D., Esper, J., Zorita, E. & Wilson, R. A noodle, hockey stick, and spaghetti plate: a perspective on high-resolution paleoclimatology. *Wiley Interdisciplinary Reviews: Climate Change* **1**, 507-516 (2010).

8 Anchukaitis, K. J. & Smerdon, J. E. Progress and uncertainties in global and hemispheric temperature reconstructions of the Common Era. *Quaternary Science Reviews* **286**, 107537 (2022).

9 Wilson, R. *et al.* Last millennium northern hemisphere summer temperatures from tree rings: Part I: The long term context. *Quaternary Science Reviews* **134**, 1-18 (2016).

10 Schneider, L. *et al.* Revising midlatitude summer temperatures back to AD 600 based on a wood density network. *Geophysical Research Letters* **42**, 4556-4562 (2015).

11 Zhao, B. *et al.* Prolonged drying trend coincident with the demise of Norse settlement in southern Greenland. *Science advances* **8**, eabm4346 (2022).

12 Bradley, R. S., Wanner, H. & Diaz, H. F. The medieval quiet period. *The Holocene* **26**, 990-993 (2016).

13 Knutti, R. & Hegerl, G. C. The equilibrium sensitivity of the Earth's temperature to radiation changes. *Nature Geoscience* **1**, 735-743 (2008).

14 Consortium, P. k. A global multiproxy database for temperature reconstructions of the Common Era. *Scientific data* **4** (2017).

15 Cook, E. R., Briffa, K. R., Meko, D. M., Graybill, D. A. & Funkhouser, G. The'segment length curse'in long tree-ring chronology development for palaeoclimatic studies. *The Holocene* **5**, 229-237 (1995).

16 Esper, J. *et al.* Orbital forcing of tree-ring data. *Nature Climate Change* **2**, 862-866 (2012).

17 Franke, J., Frank, D., Raible, C. C., Esper, J. & Brönnimann, S. Spectral biases in tree-ring climate proxies. *Nature Climate Change* **3**, 360-364 (2013).

18 Esper, J., Schneider, L., Smerdon, J. E., Schöne, B. R. & Büntgen, U. Signals and memory in tree-ring width and density data. *Dendrochronologia* **35**, 62-70 (2015).

19 Zhang, H. *et al.* Modified climate with long term memory in tree ring proxies. *Environmental Research Letters* **10**, 084020 (2015).

20 Esper, J. *et al.* Ranking of tree-ring based temperature reconstructions of the past millennium. *Quaternary Science Reviews* **145**, 134-151 (2016).

21 McCarroll, D., Young, G. H. & Loader, N. J. Measuring the skill of variance-scaled climate reconstructions and a test for the capture of extremes. *The Holocene* **25**, 618-626 (2015).

22 Büntgen, U. Scrutinizing tree-ring parameters for Holocene climate reconstructions. *Wiley Interdisciplinary Reviews: Climate Change*, e778 (2022).

23 Battipaglia, G. *et al.* Five centuries of Central European temperature extremes reconstructed from tree-ring density and documentary evidence. *Global and Planetary Change* **72**, 182-191 (2010).

24 Von Storch, H. *et al.* Reconstructing past climate from noisy data. *Science* **306**, 679-682 (2004).

25 Belmecheri, S., Babst, F., Wahl, E. R., Stahle, D. W. & Trouet, V. Multi-century evaluation of Sierra Nevada snowpack. *Nature Climate Change* **6**, 2-3 (2016).
26 Lücke, L. J., Hegerl, G. C., Schurer, A. P. & Wilson, R. Effects of memory biases on variability of temperature reconstructions. *Journal of Climate* **32**, 8713-8731 (2019).
27 Von Arx, G., Crivellaro, A., Prendin, A. L., Čufar, K. & Carrer, M. Quantitative wood anatomy—practical guidelines. *Frontiers in plant science* **7**, 781 (2016).
28 Prendin, A. L. *et al.* New research perspectives from a novel approach to quantify tracheid wall thickness. *Tree physiology* **37**, 976-983 (2017).
29 Björklund, J. *et al.* Scientific merits and analytical challenges of tree-ring densitometry. *Reviews of Geophysics* **57**, 1224-1264 (2019).
30 Björklund, J., Seftigen, K., Fonti, P., Nievergelt, D. & von Arx, G. Dendroclimatic potential of dendroanatomy in temperature-sensitive Pinus sylvestris. *Dendrochronologia* **60**, 125673 (2020).
31 Lopez-Saez, J. *et al.* Tree-Ring Anatomy Of Pinus Cembra Trees Open New Avenues for Climate Reconstructions In the European Alps. *Available at SSRN 4132985*
32 Seftigen, K. *et al.* Prospects for dendroanatomy in paleoclimatology–a case study on Picea engelmannii from the Canadian Rockies. *Climate of the Past Discussions*, 1-32 (2022).
33 Allen, K., Nichols, S., Evans, R. & Baker, P. Characteristics of a Multi-species Conifer Network of Wood Properties Chronologies From Southern Australia. *Dendrochronologia*, 125997 (2022).
34 Melvin, T. M., Grudd, H. & Briffa, K. R. Potential bias in 'updating'tree-ring chronologies using regional curve standardisation: Re-processing 1500 years of Torneträsk density and ring-width data. *The Holocene* **23**, 364-373 (2013).
35 Linderholm, H. W. & Gunnarson, B. E. Were medieval warm-season temperatures in Jämtland, central Scandinavian Mountains, lower than previously estimated? *Dendrochronologia* **57**, 125607 (2019).
36 Grudd, H. Torneträsk tree-ring width and density AD 500–2004: a test of climatic sensitivity and a new 1500-year reconstruction of north Fennoscandian summers. *Climate dynamics* **31**, 843-857 (2008).
37 Matskovsky, V. & Helama, S. Testing long-term summer temperature reconstruction based on maximum density chronologies obtained by reanalysis of tree-ring data sets from northernmost Sweden and Finland. *Climate of the Past* **10**, 1473-1487 (2014).
38 Büntgen, U. *et al.* Prominent role of volcanism in Common Era climate variability and human history. *Dendrochronologia* **64**, 125757 (2020).
39 Guillet, S. *et al.* Climate response to the Samalas volcanic eruption in 1257 revealed by proxy records. *Nature geoscience* **10**, 123-128 (2017).
40 Wu, T. *et al.* An overview of BCC climate system model development and application for climate change studies. *Journal of Meteorological Research* **28**, 34-56 (2014).
41 Landrum, L. *et al.* Last millennium climate and its variability in CCSM4. *Journal of climate* **26**, 1085-1111 (2013).
42 Dufresne, J.-L. *et al.* Climate change projections using the IPSL-CM5 Earth System Model: from CMIP3 to CMIP5. *Climate dynamics* **40**, 2123-2165 (2013).

43 Yukimoto, S. *et al.* A new global climate model of the Meteorological Research Institute: MRI-CGCM3—Model description and basic performance—. *Journal of the Meteorological Society of Japan. Ser. II* **90**, 23-64 (2012).
44 Bao, Q. *et al.* The flexible global ocean-atmosphere-land system model, spectral version 2: FGOALS-s2. *Advances in Atmospheric Sciences* **30**, 561-576 (2013).
45 Phipps, S. *et al.* The CSIRO Mk3L climate system model version 1.0–Part 1: Description and evaluation. *Geoscientific Model Development* **4**, 483-509 (2011).
46 Miller, R. L. *et al.* CMIP5 historical simulations (1850–2012) with GISS ModelE2. *Journal of Advances in Modeling Earth Systems* **6**, 441-478 (2014).
47 Giorgetta, M. A. *et al.* Climate and carbon cycle changes from 1850 to 2100 in MPI-ESM simulations for the Coupled Model Intercomparison Project phase 5. *Journal of Advances in Modeling Earth Systems* **5**, 572-597 (2013).
48 Marsh, D. R. *et al.* Climate change from 1850 to 2005 simulated in CESM1 (WACCM). *Journal of climate* **26**, 7372-7391 (2013).
49 Watanabe, S. *et al.* MIROC-ESM 2010: Model description and basic results of CMIP5-20c3m experiments. *Geoscientific Model Development* **4**, 845-872 (2011).
50 Johns, T. *et al.* Anthropogenic climate change for 1860 to 2100 simulated with the HadCM3 model under updated emissions scenarios. *Climate dynamics* **20**, 583-612 (2003).

Main manuscript Figure Legends

Figure 1. From Fennoscandian forests and lakes to quantitative wood anatomy-based tree-ring data. **a)** Map showing the general tree-sampling region (red polygon) from where instrumental temperature data and Climate model data were also extracted (Sweden – yellow and Finland – blue in color). The map was created in the Matlab computing environment using the M Map mapping package[67]. **b)** Wood sampling from living and dead trees. **c)** From the resulting high-resolution / intra-ring profiles, annual maxima, minima, latewood and earlywood values of radial cell wall thickness and anatomical density were extracted. **d)** Visualizing bands of quantitative wood anatomy data aggregation (thick black lines: tree-ring boundaries, thin black lines: 30-µm bands within a tree ring), where the colored cells are included in the final band of aggregation in the latewood. **e)** Illustration of various cell dimensions considered in this study.

Figure 2. Fennoscandian tree-ring anatomy A-FEN shows excellent warm season temperature reconstruction skill and a current climate substantially warmer than the Medieval. **a)** A-FEN, produced in this study, calibrated using regional mean air MJJA temperatures[68] (R^2 ensemble range within brackets (a = 0.05)), and corresponding results for the Fennoscandian X-ray-based data (X-FEN) dataset, from Wilson, et al. [9], using JJA temperatures. The irregular winter/spring of

1902/1903, led to a massive dieback of yearly branch-shoots in the region[55], highlighted by the yellow area. In these years with extremely narrow rings, the X-ray technique struggles to measure high maximum density values due to its comparatively lower effective measurement resolution[29] (see Extended Data Fig. 4). **b)** Replication and pairwise inter-series correlation (Rbar) of A-FEN in blue and for X-FEN in red. **c)** Centennial-scale variations (see Methods) compared between A-FEN, X-FEN, climate model simulations, and Northern Hemisphere and global temperature reconstructions. The five large-scale reconstructions[1,9,10,38,39], as well as the eleven regionally extracted climate-model simulations[40-50] are represented by probabilistic percentile ranges (grey and green shaded areas respectively). The vertical arrows highlight the overall discrepancies of the X-FEN compared to the other data.

Figure 3. The climate models and the Fennoscandian tree-ring anatomy A-FEN show unprecedented incidence of warm extremes in the past century, and comparable dynamics among Medieval and current climate. **a)** A-FEN shows that warm years are significantly overrepresented in the 20th century. In contrast, the Fennoscandian X-ray-based data (X-FEN) reveals significant overrepresentation of warm years during the MCA*. The simulations[40-50] in green shading (probabilistic percentile range based on the respective incidences) largely agree with A-FEN of significant overrepresentation of warm summers in the most recent century **b)** Climate period mean values of A-FEN, X-FEN, and the model ensemble during the Medieval (850-1100 CE) and Little Ice Age (1450-1850 CE), with the current warm period (CWP) adjusted to zero in all datasets, for ease of comparison.

Figure 4. The Fennoscandian X-ray-based data X-FEN portrays the Medival climate as significantly warmer than Fennoscandian tree-ring anatomy A-FEN. **a)** Unfiltered reconstructions with 95% confidence intervals around A-FEN based on ± 1 and 2 x standard error (SE) of the full set of trees (n = 188) included in the A-FEN dataset (i.e., not based on the subsampled A-FEN ensemble members). The mean and variance of the reconstructions are adjusted to zero and unity over the 1850-2010 overlap. **b)** Regression residuals between X-FEN and A-FEN. The Durbin-Watson statistic reveal that the residuals are far from random, underscoring the systematic and significant differences between X-FEN and A-FEN. **c)** Same as in **a)** but the data is low-pass filtered using 100-year splines.

Methods

Tree-ring material

The trees used in this study were sub-sampled from material from two distinct but proximal temperature reconstructions based on X-ray densitometry (or maximum latewood density; MXD), they are known to paleoclimatologists as the N-scan[16,20] (Finland) and the Torneträsk[34,36,69-71] (Sweden) MXD reconstructions. Data from these sites have been combined previously by Esper, et al. [2] and Matskovsky and Helama [37]. We used the arithmetic average of Esper et al and Matskovsky and Helama, developed and used in the Wilson, et al. [9] NH temperature reconstruction referred to hereafter as X-FEN, for comparisons with the QWA data, referred to as A-FEN. The sample collection of N-scan was updated in 2011 and 2014. The living-tree material from 2014 has previously been used in publications exploring wood anatomical data performance compared to other microdensitometric techniques including X-ray densitometry[29,30] (hereafter N-scan DC). The N-scan DC, analyzed using wood anatomical techniques in 2015-2017, consisted originally of 29 trees (two samples per tree). Here we randomly subsampled 10 of these trees (one sample per tree) to harmonize sample replication through time, and to match replication with the Torneträsk dataset. The N-scan DC was appended to six more living trees (sampling date 2011), as well as the original subfossil sample collection of N-scan (dead trees preserved in mountain lake sediments) [16]. The sample collection from Torneträsk was updated by sampling 14 living trees in May 2020, and this material was appended to the dry deadwood material that was previously analyzed using X-ray densitometry[69], but also to some recently collected dry deadwood samples previously analyzed only for tree-ring width[34,36]. The new wood anatomical versions of N-scan and Torneträsk comprise measurements from 99 trees (671-2013 CE) and 89 trees (545-2019 CE), respectively, for a total of 188 trees. The combined dataset contains around 10 trees per year from each collection, amounting to a total sample replication of 20-30 trees per year for the period 850-2019 CE (Fig. 2). The latest versions of the X-ray based Torneträsk MXD and N-scan MXD consist of 124 (441-2010 CE), and 294 trees (138 BC – 2006 AD), respectively, for a total of 418 trees.

Quantitative wood anatomical data production

The wood anatomical analyses were made following state-of-the-art techniques[27], but with adjustments to protocols for more recently analyzed subset members.

411 The thin sections from the N-scan DC samples were cut to a thickness of c. 15 µm using a sledge
412 microtome[72] equipped with Feather N35 disposable blades (Feather Safety Razor Co., Ltd., Osaka,
413 Japan). Images of the sections were serially captured with a camera (Canon EOS 650D, Canon
414 Inc., Tokyo, Japan) mounted on a microscope (Olympus BX41, Olympus Corp., Tokyo, Japan) at
415 a resolution of 2.36 pixels μm^{-1}. Composite images of the sections were created using PTGui (New
416 House Internet Services B.V., Rotterdam) stitching software. The second N-scan component was
417 produced at the University of Padova, hereafter N-scan Padova and constitute half of the full-
418 length N-scan (including 6 living trees). These samples were cut to thin sections with a Leica RM
419 2255 rotary microtome (Leica, Heidelberg, Germany) to c. 15 µm thickness, digitized using a
420 camera (Nikon Eclipse 80i, Nikon, Tokyo, Japan) connected a light microscope and then stitched
421 using PTGui (v8.3.3, New House Internet Services B.V., Rotterdam, The Netherlands). The
422 remaining N-scan component comprising half of the subfossil material were developed using the
423 latest protocol at WSL (hereafter N-scan WSL). Each wood sample was cut into c. 2.5-cm long
424 pieces and embedded in paraffin using an embedding station (Leica TP1020 combined with Leica
425 HistoCore Arcadia, Leica, Heidelberg, Germany). Thin sections of 12 µm thickness were produced
426 using a Leica RM2245 rotary microtome (Leica, Heidelberg, Germany), and images were captured
427 with a Zeiss Axioscan.Z1 slide scanner (Carl Zeiss AG, Germany) at a resolution of 2.27
428 pixels μm^{-1}.
429 The entire Torneträsk dataset was produced using the latest WSL protocol. Regardless of cutting
430 and image capturing protocol, each thin section was double-stained with safranin and astrablue to
431 increase contrast, then permanently fixed with Eukitt, Canada balsam or Euparal. The software
432 ROXAS (v3.1) was used to automatically detect anatomical structures of all tracheid cells[28,73] (75–
433 100 radial files per ring), as well as annual ring borders (Fig. 1). The latewood in each ring was
434 defined using a Mork's index value greater than 1. That is, those tangential cell bands where twice
435 the double cell wall thickness was larger than the lumen diameter across the radial direction on
436 average, were defined as latewood[74]. The total QWA dataset comprises c. 50 million tracheid cell
437 measurements. For more details on the anatomical data extraction see Björklund, et al. [30].
438
439 *Chronology development*
440 We used the "delta radial cell wall thickness" parameter as the single parameter for our A-FEN
441 reconstruction. This parameter represents the difference between radial cell wall thickness in the

latewood and earlywood, specifically [maximum radial cell wall thickness – minimum radial cell wall thickness]. This parameter was chosen among a range of parameters, such as maximum, latewood and delta[75] radial cell wall thickness, maximum and delta anatomical density[29], as well as tangential latewood lumen diameter and latewood width. These parameters all contain very pronounced and almost identical temperature signals, where the delta radial cell wall thickness overall performs the best (Extended Data Fig. 2). All considered parameters were subjected to standardization/detrending using the widely adopted Regional Curve Standardization approach[71]. This technique is used to preserve as much long-term climate variability as the included samples permit[15]. The methodology has been fine-tuned over many years, but without having changed considerably[54], at least when using multi-generational and replication-balanced datasets through time. Therefore, we used the classic single-RCS approach (one regional curve for all parameter samples), following the principle of parsimony. In the following we specify how we implemented the approach. 1) Each collection was subsampled to a sample replication <12 through time by randomly removing trees from potentially oversampled periods, and then aligning all the chosen trees by the pith year (pith offsets were estimated and used). 2) One regional average curve was calculated as the arithmetic mean of all included trees per pith year, then it was 3) fitted with a series of customized functions to estimate a smooth growth curve, or the Regional Curve (RC). 3a) A cubic smoothing spline with a frequency cut-off of 50% at 50 years was fitted to the regional average. 3b) The cambial age at which the sample replication of the age-aligned samples was lower than 10 trees was determined. 3c) From this point and 20 years back, a mean value was calculated and appended to the 50-year spline from the replication threshold until the final year of the oldest tree. 3d) At around 50 years of cambial age, the trees have passed the juvenile phase and entered the mature phase which generally display a modest decline in growth values. From 50 years and onwards, a cubic smoothing spline with a frequency cut-off of 50% at 500 years was fitted and appended to the 1 to 50 year segment of the 3a RC function. 3e) Finally, a cubic smoothing spline with a frequency cut-off of 50% at 50 years was fitted to the whole 3d) function. The steps 1-3e were repeated 100 times and a mean of all 100 RC's was calculated forming the final and only RC per chronology. This RC was subtracted from the complete sets of measurements to create dimensionless tree-ring indices. Ratios were used for ring width and latewood widths.

We also developed datasets without idiosyncratic signal processing (that is, no RCS applied), to understand how much the RCS changed the obtained results. Although the detrended data exhibit

very little difference compared to non-detrended data, we use the detrended version because of obvious juvenile trends (from c. 0-20 years) in the raw anatomical data parameters.

Because we used datasets developed under a step-wise progression of measurement protocols (relevant only for N-scan), we examined the different components for discrepancies in means and variances, which are critical for the appropriate implementation of RCS. We found inconsistencies, and accordingly harmonized the data based on a concurrent overlap between each N-scan component of >5 samples. Therefore, we first calculated the mean and variance of the N-scan Padova component during the >5 sample replication overlap with the N-scan DC component (only living trees). Then we forced the N-scan DC component to take on the mean and variance of the N-scan Padova component. Thereafter, we repeated the operation with the N-scan WSL component, again using N-scan Padova as target. These operations were done prior to RCS due to relatively low, and sometimes uneven temporal distribution in replication of each component.

Torneträsk and N-scan were processed using separate RCs, and subsequently their means and variances were adjusted to zero and unity on the 850-2005 CE overlap and all indices were pooled into the A-FEN dataset. After this, the A-FEN dataset was subsampled into an ensemble of 100 datasets by means of random sampling (without replacement) aimed at a consistent replication of 15 trees/year for the full length of each dataset. This operation was employed to reveal the stability of temperature signals and lower frequency variations through time as a function of changes in included trees. Moreover, creating distributions of datasets allowed us to assess if the obtained results for A-FEN and X-FEN were significantly distinct from each other in any respect.

Climate Model ensemble

Simulations from 11 models (BCC-CSM1-1[40], CCSM4[41], IPSL-CM5A-LR[42], MRI-CGCM3[43], FGOALS-s2[44], CSIRO Mk3L[45], GISS E2 R[46], MPI ESM P[47], CESM1[48], MIROC ESM[49], HadCM3[50]) contributing to the Coupled and Paleo Model Intercomparison Projects Phases[51,76] (CMIP5–PMIP3) were used in the model/proxy comparison. The choice of models was based on the criteria of having essentially complete monthly surface air temperature variables covering the past millennium (850–1849 CE) and the historical period (1850–2005 CE). The *past1000* simulations were forced using reconstructed solar, volcanic, greenhouse gas (GHG) and aerosol forcings, and partly land use changes, whereas the historical simulations included natural and anthropogenic forcings[51,76]. Monthly values of May, June, July and August (MJJA) temperatures

were extracted from the land area bound by latitudes 65-70° N, and longitudes 15-30° E. A simple monthly arithmetic mean was calculated to directly correspond to the best fit instrumental target season for the proxy data. Most analyses executed for the proxy data were performed also for the models after they were normalized to a mean of zero and a standard deviation of unity over the period 850-2005 CE.

Proxy calibration/Temperature signals

The association with temperature was determined using Pearson correlations with monthly data from HadCRUT5[68] (5° gridded monthly dataset, Lat. 65-70° N, Lon. 15-30° E). Coefficients of determination (R^2) were calculated for three non-overlapping periods (i.e. 1850-1900, 1901-1960 and 1961 to the final year of each dataset) to check the stability in the best fit target season MJJA for A-FEN and JJA for X-FEN. The A-FEN reconstruction was further validated using the Reduction of Error (RE) and Coefficient of Efficiency (CE) statistics[77]. The simple non-parametric test referred to as "Extreme Value Capture"[21] was used to determine how well each datasets reflect both cold and warm extremes of the instrumental dataset. That is, the number of the correctly reconstructed extreme years 'captured' beyond the thresholds defined by the upper and lower 10% of the measured temperature data (Extended Data Fig. 1). The calibration results were calculated for both RCS-processed (Fig. 2 and Extended Data Tab. 1) and non-detrended datasets (Extended Data Fig. 3). High-pass filtered datasets (using cubic smoothing splines[78] with 50% frequency response cut-off at 40 years), untreated, and low-pass filtered (using cubic smoothing splines[78] with 50% frequency response cut-off at 5 and 10 years) were also used for the monthly temperature correlations. All correlations were adjusted for loss of degrees of freedom depending on the autocorrelation in each series[79]. The reconstructions and models were compared by scaling each dataset to a mean of zero and standard deviation of unity over the period 850-2005 CE. The large-scale reconstructions[1,9,10,38,39] were scaled *after* smoothing to the mean and variance of the smoothed X-FEN to facilitate comparisons.

The pine tree canopy damage

In the winter/spring of 1902/1903, an extra-growing season trauma afflicted many pine trees in north and central Sweden, described by Gunnar Andersson of the Governmental Forest Research Institution in 1905[55]. Several references therein reveal that the unusual event was also noticed in

Norway, and as far east as the Kola peninsula. In brief, the growing season of 1902 was cold and wet, and the radial growth and cell dimensions underdeveloped. In mid-September 1902, heavy wet snow fell and accumulated onto the trees. A few days later, temperatures drastically dropped to nearly -10° C, leading to damaged or broken branches of the trees. In the spring of 1903, unusual warmth early in the season was followed by icy cold and dry winds from the east, leaving pine shoots stunted. This arguably led to reduced canopy photosynthetic capacity[56], with persistent reductions in wood cell divisions, resulting in extremely narrow ring widths for up to 6 years. The significance of this episode relates to the temporary collapse of ring-width expansion foremost controlled by climate, while individual cell dimensions appear largely unaffected. If cell dimensions continue to form under dominant control of climate, this would theoretically imply that MXD, which is also predominantly a function of cell dimensions[29], would be indifferent to the canopy damage as well. Instead, MXD values appear suppressed for several years, implying that MXD measurements may be affected by the extremely narrow rings characterizing this episode. For interested readers not fluent in Swedish, we share some excerpts loosely translated to English from the original reference[55].

"Anyone travelling to the North in the summer of 1903 could not fail to observe, especially in younger pine stands, that individual shoots, or the entire upper shoot systems, had withered away. Here and there, especially in certain areas, the stands were rather badly ravaged and their appearance attracted the attention of both foresters and to a large extent laymen as well."

"A condition which many forest district administrators paid attention to was the unusual development of the 1902 years yearly shoot. On the one hand the shoots were abnormally long, and on the other, poorly developed. Sometimes the length was more than double that of the shoots the preceding summer of 1901, but the pine needles were short and lay snug onto the yearly shoot, different from what is usually the case in fully mature shoots late in the fall."

"Several opinions were raised that the direct cause of the pine shoot damage was the period of warm temperatures followed by icy cold that occurred in April 1903. April experienced summer warmth that was believed to have triggered the sap flow in the trees. Thereafter followed a grim late winter with large snow masses. Many acquired the opinion that the pine shoot damage was

caused by the too early commencement of processes in the tissues in the spring of 1903, and that they later suffered dehydration from the physiologically cold and dry period. These people also emphasize the unusually hardened ground frost and the long time it took to thaw, as an exacerbating circumstance for the trees to absorb water from the ground."

"Microscopic investigations of 1902 years tree ring revealed that it was narrower than 1901 and that the cells in the wood were smaller and the cell walls were thinner, with a more pronounced resin content in the wood cells. For example, the tangential width was 0.0138 mm in 1902 and 0.0179 mm in 1901."

It is interesting that about hundred years after these keen observations to confirm that the starting point of the pine tree canopy damage was marked by so-called "blue-rings" [80] in 1902. In double stained microsections of wood, using safranin and astra-blue, the cell walls appear blue in color because of markedly reduced lignification of the cell walls. A normally lignified cell wall should be colored red from the safranin. The observations from Andersson[55] testifies that the conditions for the trees in this period were unusually harsh, and perhaps the combination of the underdeveloped wood formed during the very cold 1902 was more vulnerable to the late season cold-spell in September, and hence the blue-ring was the outcome.

Full-length dataset assessments

The common signal among trees for each specific tree-ring parameter was established using the Rbar statistic[53] (the mean pairwise correlation of all trees overlapping in time) using a moving window of 100 years with a lag of 10 years across the full period. A high Rbar value indicates that the trees in a tree-ring chronology responds similarly to environmental forcing). Using the moving window Rbar and tree replication through time, the statistic Expressed Population Signal[53] (EPS) was calculated to gauge the robustness of each dataset (both A-FEN and X-FEN exhibited EPS of above 0.85 for the full 850-present periods). The Rbar and replication for X-FEN was done using the series included in Matskovsky and Helama [37]. The uncertainty of A-FEN was calculated using ± 1 and 2 x standard error (SE; standard deviation of the annual spread of values divided by the square root of the annual tree replication). The difference between X-FEN and A-FEN was evaluated by examining their regression residuals using the Durbin-Watson statistic. We assessed

the spectral characteristics of the proxy and model data using the Thomson's multitaper method[81], applied with four windows, to transform the records from the time to the frequency domain within the MATLAB function pmtmPH.m[82]. We used a superposed epoch analysis[83] (SEA) to evaluate the degree of cooling associated with volcanic aerosol forcing in the models, and corresponding cooling in the proxies. The variant of the SEA was inspired by Brad Adams, et al. [84] and the computing was done in MATLAB using the function developed in Blarquez and Carcaillet [85]. We compiled event lists from Gao, et al. [86], consisting of the 10 and the 30 largest (based on sulfate aerosol injection) northern Hemisphere events. We used only Gao et al as basis for the event lists because most models in our ensemble were forced with Gao et al. We employed a model ensemble mean in the SEA, to explore the degree of volcanic cooling the models express. The incidence of warm extremes was quantified by first extracting the 100 warmest years from the common overlap 850-2005 CE of each simulation and reconstruction. The extracted extremes were then summed per century and compared with confidence intervals based on number of extremes happening by chance. Confidence intervals were calculated by generating 1000 synthetic time series over the interval 850-2005 CE using 1) random white noise processes, and 2) colored noise processes with a beta-coefficient of 0.5 (beta coefficients white noise = 0, pink noise = 1 for reference), and then taking the 97.5th percentile as confidence limit.

Data availability Statement

The A-FEN reconstruction will be available on the National Centers for Environmental Information on the NOAA homepage https://www.ncei.noaa.gov/access/paleo-search/?dataTypeId=3. The data used in the reconstruction will be made available at NOAA International Tree Ring Data Bank. The data used to perform our analysis as well as our results are uploaded to Zenodo and are accessible using the following link: (Will be created once the manuscript publication date is determined).

Code Availability Statement

The codes that support the findings of this study are available alongside Source Data on the Zenodo repository and can be accessed using the following link: (Will be created once the manuscript publication date is determined).

Methods References

51 Taylor, K. E., Stouffer, R. J. & Meehl, G. A. An overview of CMIP5 and the experiment design. *Bulletin of the American meteorological Society* **93**, 485-498 (2012).

52 Braconnot, P. *et al.* Evaluation of climate models using palaeoclimatic data. *Nature Climate Change* **2**, 417-424 (2012).

53 Wigley, T. M., Briffa, K. R. & Jones, P. D. On the average value of correlated time series, with applications in dendroclimatology and hydrometeorology. *Journal of Applied Meteorology and Climatology* **23**, 201-213 (1984).

54 Helama, S., Melvin, T. M. & Briffa, K. R. Regional curve standardization: State of the art. *The Holocene* **27**, 172-177 (2017).

55 Andersson, G. Om talltorkan i öfra Sverige våren 1903. *Meddelanden från statens skogsförsöksanstalt* **2** (1905).

56 Pallardy, S. G. *Physiology of woody plants*. (academic press, 2010).

57 Vaganov, E. A., Hughes, M. K. & Shashkin, A. V. *Growth dynamics of conifer tree rings: images of past and future environments*. Vol. 183 (Springer Science & Business Media, 2006).

58 Abbott, P. M. *et al.* Cryptotephra from the Icelandic Veiðivötn 1477 CE eruption in a Greenland ice core: confirming the dating of volcanic events in the 1450s CE and assessing the eruption's climatic impact. *Climate of the Past* **17**, 565-585 (2021).

59 Stoffel, M. *et al.* Estimates of volcanic-induced cooling in the Northern Hemisphere over the past 1,500 years. *Nature Geoscience* **8**, 784-788 (2015).

60 Anchukaitis, K. J. *et al.* Last millennium Northern Hemisphere summer temperatures from tree rings: Part II, spatially resolved reconstructions. *Quaternary Science Reviews* **163**, 1-22 (2017).

61 McCarroll, D. *et al.* A 1200-year multiproxy record of tree growth and summer temperature at the northern pine forest limit of Europe. *The Holocene* **23**, 471-484 (2013).

62 Neukom, R. *et al.* Inter-hemispheric temperature variability over the past millennium. *Nature climate change* **4**, 362-367 (2014).

63 González Rouco, J. F. Continental-scale temperature variability in PMIP3 simulations and PAGES 2k regional temperature reconstructions over the past millennium. *Climate of the Past* **11**, 1673-1699 (2015).

64 Lorenz, E. N. Deterministic nonperiodic flow. *Journal of atmospheric sciences* **20**, 130-141 (1963).

65 D'Arrigo, R., Wilson, R., Liepert, B. & Cherubini, P. On the 'divergence problem'in northern forests: a review of the tree-ring evidence and possible causes. *Global and planetary change* **60**, 289-305 (2008).

66 Büntgen, U. *et al.* The influence of decision-making in tree ring-based climate reconstructions. *Nature communications* **12**, 1-10 (2021).

67 M_Map: A mapping package for MATLAB (2020).

68 Morice, C. P. *et al.* An updated assessment of near-surface temperature change from 1850: The HadCRUT5 data set. *Journal of Geophysical Research: Atmospheres* **126**, e2019JD032361 (2021).

69 Schweingruber, F. H., Bartholin, T., Schaur, E. & Briffa, K. R. Radiodensitometric-dendroclimatological conifer chronologies from Lapland (Scandinavia) and the Alps (Switzerland). *Boreas* **17**, 559-566 (1988).
70 Briffa, K. R. *et al.* A 1,400-year tree-ring record of summer temperatures in Fennoscandia. *Nature* **346**, 434-439 (1990).
71 Briffa, K. R. *et al.* Fennoscandian summers from AD 500: temperature changes on short and long timescales. *Climate dynamics* **7**, 111-119 (1992).
72 Gärtner, H., Lucchinetti, S. & Schweingruber, F. A new sledge microtome to combine wood anatomy and tree-ring ecology. *IAWA journal* **36**, 452-459 (2015).
73 von Arx, G. & Carrer, M. ROXAS–A new tool to build centuries-long tracheid-lumen chronologies in conifers. *Dendrochronologia* **32**, 290-293 (2014).
74 Denne, M. P. Definition of Latewood According to Mork (1928). *IAWA Journal* **10**, 59-62 (1989). https://doi.org:https://doi.org/10.1163/22941932-90001112
75 Björklund, J., Gunnarson, B. E., Seftigen, K., Esper, J. & Linderholm, H. Blue intensity and density from northern Fennoscandian tree rings, exploring the potential to improve summer temperature reconstructions with earlywood information. *Climate of the Past* **10**, 877-885 (2014).
76 Schmidt, G. *et al.* Climate forcing reconstructions for use in PMIP simulations of the Last Millennium (v1. 1). *Geoscientific Model Development* **5**, 185-191 (2012).
77 National Research Council. *Surface temperature reconstructions for the last 2,000 years*. (National Academies Press, 2007).
78 Cook, E. R. & Peters, K. The smoothing spline: a new approach to standardizing forest interior tree-ring width series for dendroclimatic studies. (1981).
79 Matalas, N. C. Statistical properties of tree ring data. *Hydrological Sciences Journal* **7**, 39-47 (1962).
80 Piermattei, A., Crivellaro, A., Carrer, M. & Urbinati, C. The “blue ring”: anatomy and formation hypothesis of a new tree-ring anomaly in conifers. *Trees* **29**, 613-620 (2015).
81 Percival, D. B. & Walden, A. T. *Spectral analysis for physical applications*. (cambridge university press, 1993).
82 pmtmPH.m (MATLAB Central File Exchange, 2022).
83 Haurwitz, M. W. & Brier, G. W. A critique of the superposed epoch analysis method: its application to solar–weather relations. *Monthly Weather Review* **109**, 2074-2079 (1981).
84 Brad Adams, J., Mann, M. E. & Ammann, C. M. Proxy evidence for an El Nino-like response to volcanic forcing. *Nature* **426**, 274-278 (2003).
85 Blarquez, O. & Carcaillet, C. Fire, fuel composition and resilience threshold in subalpine ecosystem. *PLoS One* **5**, e12480 (2010).
86 Gao, C., Robock, A. & Ammann, C. Volcanic forcing of climate over the past 1500 years: An improved ice core-based index for climate models. *Journal of Geophysical Research: Atmospheres* **113** (2008).
87 Toohey, M. & Sigl, M. Volcanic stratospheric sulfur injections and aerosol optical depth from 500 BCE to 1900 CE. *Earth System Science Data* **9**, 809-831 (2017).

Acknowledgments

This work has been funded by a grant from the Swiss National Science Foundation awarded to G.v.A, supporting JB, KS, MF and SK (Project XELLCLIM no. 200021_182398). MS, PF and JB received funding from the SNF Sinergia project CALDERA (no. 183571). JE received funding from the ERC Advanced grant MONOSTAR (AdG 882727). We thank Eva Rocha for assistance with Torneträsk samples from the Dendrolab at Stockholm University. We are grateful to Samuli Helama that made us aware of the early 20th century publication of Andersson [55], describing the Pine tree canopy damage. We acknowledge the work of Mauri Timmonen and Ulf Büntgen who were involved in sampling of the dead wood material for the N-scan site.

Author Contributions

JB, GvA, KS and MC conceptualized the study. HåG, BEG, JE, MC, EP, DN conducted the field works and provided physical samples for the wood anatomical analyses. GvA, MC, MF, SK, EP coordinated, processed and measured the wood anatomical data. JB and KS performed the analyses with input from HuG, GvA, PF, DCF and MS. JB wrote the manuscript and all authors have reviewed and helped to revise the manuscript.

Author Information

Competing Interest Statement

Authors declare that they have no competing interests.

Correspondence and requests for materials should be addressed to Jesper Björklund.

Extended Data Legends

Extended Data Figure 1. Evaluation of the ability of the A-FEN and X-FEN reconstructions to capture extremes in climate targets. The instrumental temperature data was sorted from coldest to warmest and plotted together with the reconstruction values of the corresponding years. The grey boxes are bound by the 10% coldest and warmest years, and the 10th and 90th percentile of the zscore temperatures, respectively. If an extreme reconstruction value is found within the grey box, the extreme is defined as “captured”. The sum of the captured values divided by the potential sum values, is calculated and presented as a percentage of extreme value capturing. In McCarroll, et al. [21], a significance testing was implemented, and for 160-170 years of climate data, $p < 0.001$ is

745 achieved if more than 40% of values are captured. **a)** A-FEN's ability to capture JJA temperature
746 extremes. **b)** X-FEN's ability to capture JJA temperature extremes. **c)** and **d)** show same analysis
747 as **a)** and **b)** but using the target MJJA. Both datasets thus display significant amounts of extremes
748 captured, but the A-FEN captures significantly more than the X-FEN for the MJJA target season.
749 The X-FEN captures a higher percentage of cold extremes if the MJJA target season is used but
750 the same percentage of warm extremes regardless of target season. The rationale for using MJJA
751 as the target season for X-FEN is thus less clearcut than for the A-FEN. JJA is the target season
752 used in the publications originally presenting the MXD data[2,37] and is thus used in the main text
753 for the other comparisons.
754
755 **Extended Data Figure 2**. Monthly climate correlations across a range of frequency domains. **a)**
756 high-pass filtered data (cubic smoothing splines with 50 % frequency response cut-off at 40 years
757 (HP40yrs)) correlated with identically treated temperature data. **b)** RCS detrended data correlated
758 with untreated temperature data. **c)** low-pass filtered data (LP5yrs), and **d)** (LP10yrs), correlated
759 with identically treated temperature data, respectively. The monthly temperature data were
760 retrieved from HadCRUT5[68] (5° gridded monthly dataset, Lat. 65-70° N, Lon. 15-30° E).
761 Correlation coefficients in white are significant at $p < 0.01$, and black coefficients are insignificant.
762 When 10-year low-pass filtered data are used, the autocorrelation is so high that it is impossible to
763 detect significance after adjusting for loss of degrees of freedom[79], why it is meaningless to
764 continue the analysis over even lower frequencies. The parameters or reconstructions reside on the
765 y-axis, and each monthly temperature or monthly target season on the x-axis. First order
766 autocorrelation, AR(1), of the JJA and MJJA temperatures are given on top of each panel as a
767 reference, and the tree-ring parameter AR(1) can be found in the right margin of each panel. The
768 period of analysis covers the full length-overlap between all datasets (1850-2019 for anatomical
769 parameters and 1850-2006 for the X-FEN). The results are very similar if the 1850-2006 period is
770 used for the QWA data. The delta radial cell wall thickness (DeltaCWTRAD) parameter was
771 established as predictor for the A-FEN reconstruction due to overall performance in the analysis.
772
773 **Extended Data Figure 3.** Warm-season temperature reconstruction skill of A-FEN and X-FEN,
774 as well as comparisons with existing large-scale reconstructions and regional climate simulations
775 but using QWA data that has **not** been detrended using the RCS approach. The non-QWA

datatypes are identical to Figure 2 of the Main manuscript and the vertical arrows have the exact positions and dimensions as in Figure 2 for reference. **a)** A-FEN (produced in this study) calibrated using regional mean air MJJA temperatures[68] (R^2 ensemble range within brackets (a = 0.05)), and results for the X-FEN (from Wilson, et al. [9]) using corresponding JJA temperatures. The irregular winter/spring of 1902/1903, led to a massive dieback of yearly branch-shoots in the region[55], highlighted by the yellow area. In these years with extremely narrow rings, the X-ray technique struggles to measure high MXD values due to its comparatively lower effective measurement resolution[29] (see Extended Data Fig. 4). **b)** Replication and pairwise inter-series correlation (Rbar) of A-FEN in blue and the X-FEN in red. **c)** Centennial-scale variations (see Methods) compared between A-FEN, X-FEN, climate model simulations, and NH and global temperature reconstructions. The five large-scale reconstructions[1,9,10,38,39], as well as the eleven regionally extracted climate-model simulations[40-50] are represented by probabilistic percentile ranges. The vertical arrows highlight the overall discrepancies of the X-FEN compared to the other data.

Extended Data Figure 4. Illustration of the issue with comparatively low measurement resolution for X-ray MXD. **a)** X-ray image with analysis track path indicated within the solid white rectangle, and examples of the effect of different effective measurement resolutions. **b)** The photosensors in a) build up measurement profiles, where the blue sensor builds the blue profile corresponding to a 20-micron effective measurement resolution, and the orange sensor builds up the orange profile corresponding to a 60 micron effective measurement resolution, approximating the effective measurement resolution of the X-ray methodology [29]. Note how the time series of MXD reflect inverse variations if developed using high-resolution or low-resolution equipment. The explanation for this is that very narrow latewood widths are associated with comparatively lower MXD values even though the "true" MXD value may be high. **c)** Relationships between TRW and A-FEN and **d)** LWW and A-FEN. **e)** Relationships between TRW and anatomical MXD (MXDCWT) and **f)** LWW and MXDCWT. **g)** Relationships between TRW and X-FEN and **h)** LWW and X-FEN. All datasets display correlations and using datapoints covering 850-2005 CE. Note how the X-FEN always is stronger correlated with TRW and LWW than the MXDCWT. A higher correlation is expected if TRW or LWW is affecting the measurement. Spearman rank correlation coefficients were used due to the possibly non-linear relationships between width and

density. R_{raw} and $r_{diff.}$ refers to untreated and first differenced data prior to correlations, respectively.

Extended Data Figure 5. Moving window correlation coefficients revealing that X-ray MXD exhibits a stronger relationship with ring width and latewood width than anatomical MXD. Ring width (TRW) versus anatomical MXD (MXDCWT) and X-FEN, as well as latewood width (LWW) versus MXDCWT and X-FEN. Spearman rank correlations were used on RCS-detrended chronologies with a 100-year base-lengths and 10-year overlaps. For the anatomical MXDCWT data, 100 sub-sampled chronologies with 15 trees/year were used to create ensemble ranges represented in blue shades. Deviations from these blue shaded areas represent significant differences ($p < 0.05$) from the TRW and LWW correlations with MXDCWT, respectively. The X-FEN correlations often reside outside the blue areas, and at higher correlations with TRW and LWW respectively, indicating occasionally stronger dependence of X-FEN on these parameters.

Extended Data Figure 6. Comparison of A-FENs complete set of ensemble members with X-FEN. RCS-detrended A-FEN (data from this study) versus the X-FEN (data from Wilson, et al. [9]), smoothed using cubic smoothing splines with 50 % frequency response cut-off at 100 years. Note that no A-FEN ensemble member exhibit the protracted warmth during the MCA and the relatively low temperatures during the CWP, as does the X-FEN.

Extended Data Figure 7. Comparison of A-FEN versus a network of millennium-long Fennoscandian MXD datasets showing the wide range of medieval estimates and comparably modest modern warming. The MXD based temperature reconstructions from Fennoscandia are retrieved from Wilson, et al. [9], Schneider, et al. [10] and McCarroll, et al. [61] represented by a probabilistic percentile range.

Extended Data Figure 8. Spectral properties and first order autocorrelation of the reconstructions and models compared in this study. **a)** Spectral properties of the A-FEN ensemble and X-FEN on the backdrop of the model ensemble range, as well as the range of a 1000 timeseries, of equal length to the A-FEN, of colored noise with a beta coefficient of 0.5. (Beta coefficient for White

noise = 0, Pink noise = 1). **b)** Running autocorrelations AR(1) calculated for 100-year window lengths, shifted by 10-year lags.

Extended Data Figure 9. Superposed epoch analysis and comparisons over individual eruption years for the A-FEN ensemble, X-FEN and the model ensemble. SEA's using Gao, et al. [86] event lists of the 10 **a)** and 30 **b)** of the largest (based on sulfate aerosol injection) northern Hemisphere events. The model simulations were all extracted from the corresponding grid cells Lat 65-70° N, Lon 15-30° E. We used only Gao et al as basis for the event lists because most models in our ensemble were forced with Gao et al, but note that this list may not be optimal for some models and the tree-ring data. We employed a model ensemble mean in the SEA, to explore the degree of volcanic cooling the models express. **c-h)** Proxy vs model response to some specific major volcanic events dated according to Toohey and Sigl [87]. The responses to U.E. 1453 CE, Huaynaputina and Eldgjá are pronounced in the proxy data but not in the models. The responses to Samalas and Tambora are pronounced in the models but not in the proxy data. The response to Parker is present in both models and proxy.

Extended Data Table 1 Reconstruction statistics for Fennoscandian tree-ring anatomy A-FEN. Reconstruction statistics were calculated using May-August from HadCRUT5[68] (5° gridded monthly dataset, Lat. 65-70° N, Lon. 15-30° E). The reconstruction statistics were calculated over three split calibration/validation periods.

Fig. 1

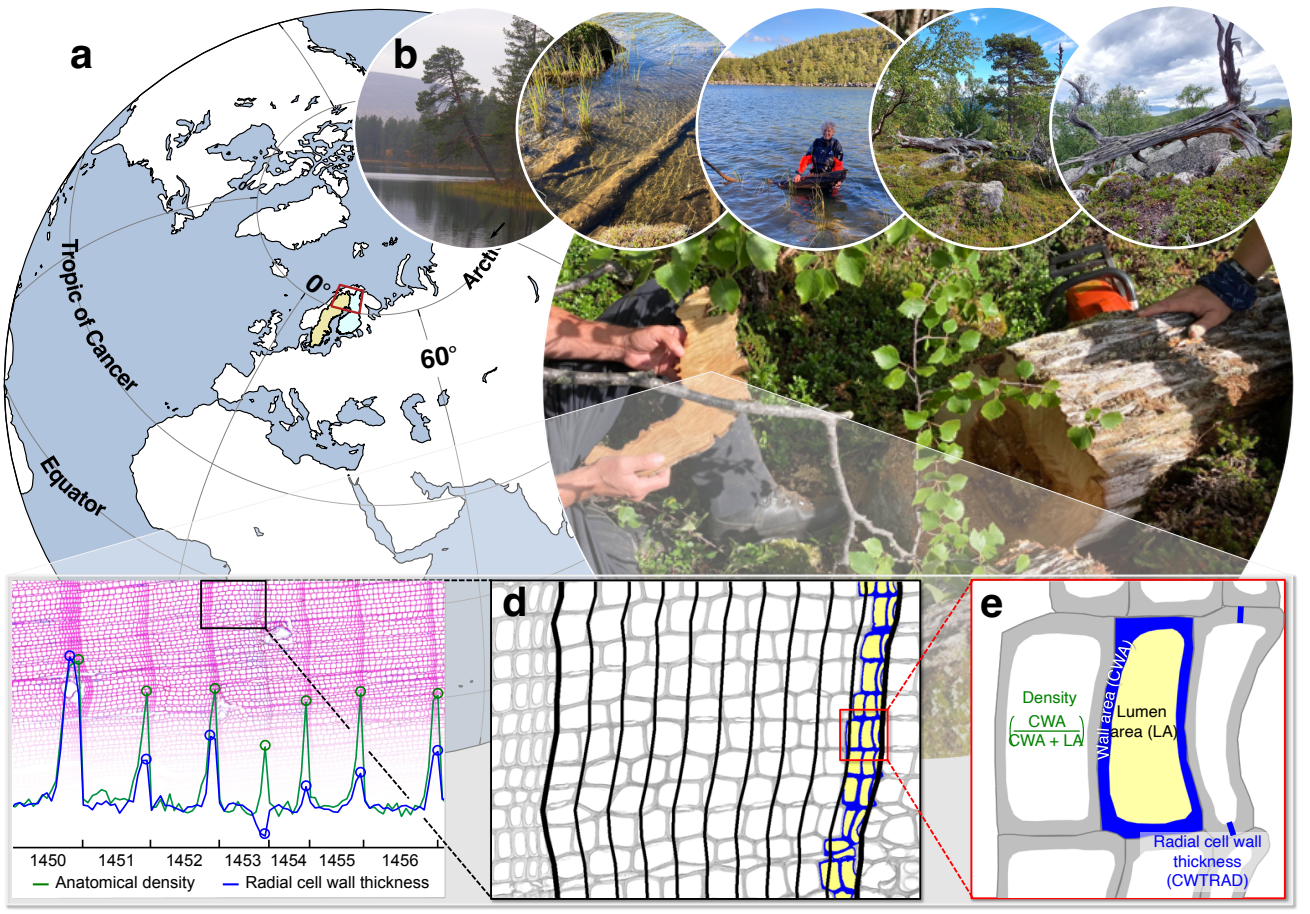
a
b
Tropic of Cancer
Equator
0°
60°
d
e
1450
1451
1452
1453
1454
1455
1456
Anatomical density
Radial cell wall thickness
Density
CWA
CWA + LA
Wall area (CWA)
Lumen
area (LA)
Radial cell wall
thickness
(CWTRAD)

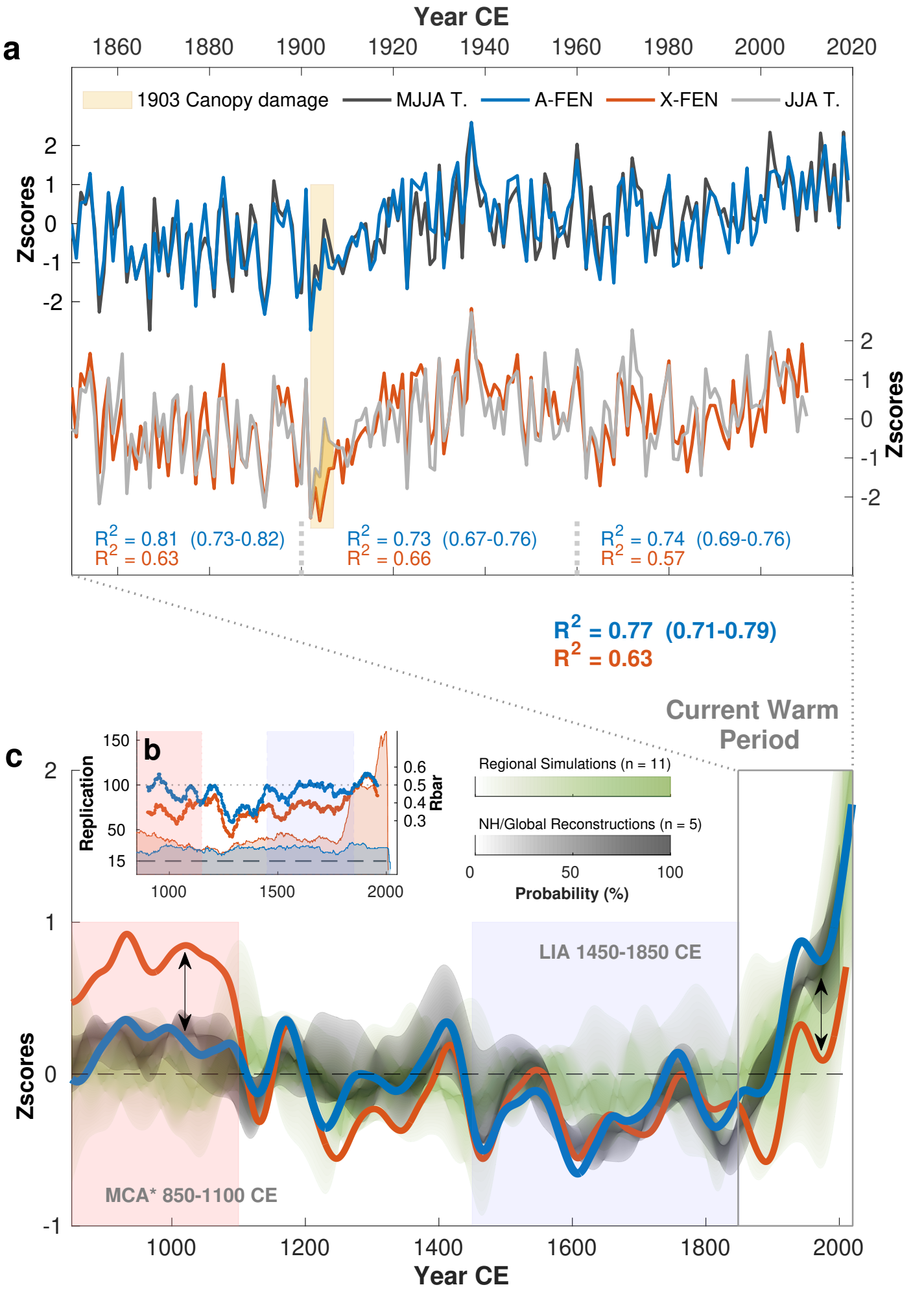
a
Year CE
1860
1880
1900
1920
1940
1960
1980
2000
2020
1903 Canopy damage
MJJA T.
A-FEN
X-FEN
JJA T.
Zscores
2
1
0
-1
-2
R^2 = 0.81 (0.73-0.82)
R^2 = 0.63
R^2 = 0.73 (0.67-0.76)
R^2 = 0.66
R^2 = 0.74 (0.69-0.76)
R^2 = 0.57
R^2 = 0.77 (0.71-0.79)
R^2 = 0.63
Current Warm Period
c
b
Replication
150
100
50
15
Rbar
0.6
0.5
0.4
0.3
1000
1500
2000
Regional Simulations (n = 11)
NH/Global Reconstructions (n = 5)
0
50
100
Probability (%)
LIA 1450-1850 CE
MCA* 850-1100 CE
1000
1200
1400
1600
1800
2000
Year CE

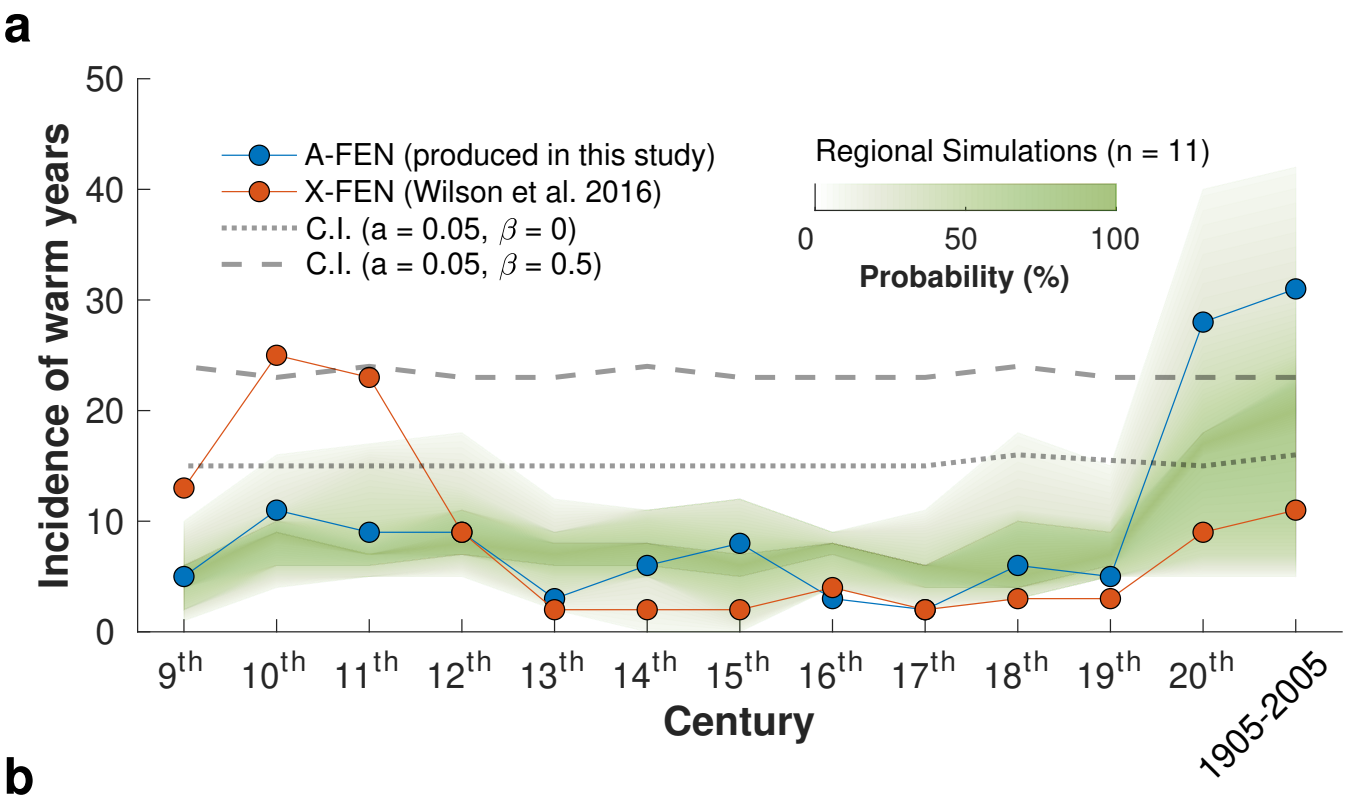
a
Incidence of warm years
50
40
30
20
10
0
A-FEN (produced in this study)
X-FEN (Wilson et al. 2016)
C.I. (a = 0.05, β = 0)
C.I. (a = 0.05, β = 0.5)
Regional Simulations (n = 11)
0
50
100
Probability (%)
9th
10th
11th
12th
13th
14th
15th
16th
17th
18th
19th
20th
1905-2005
Century

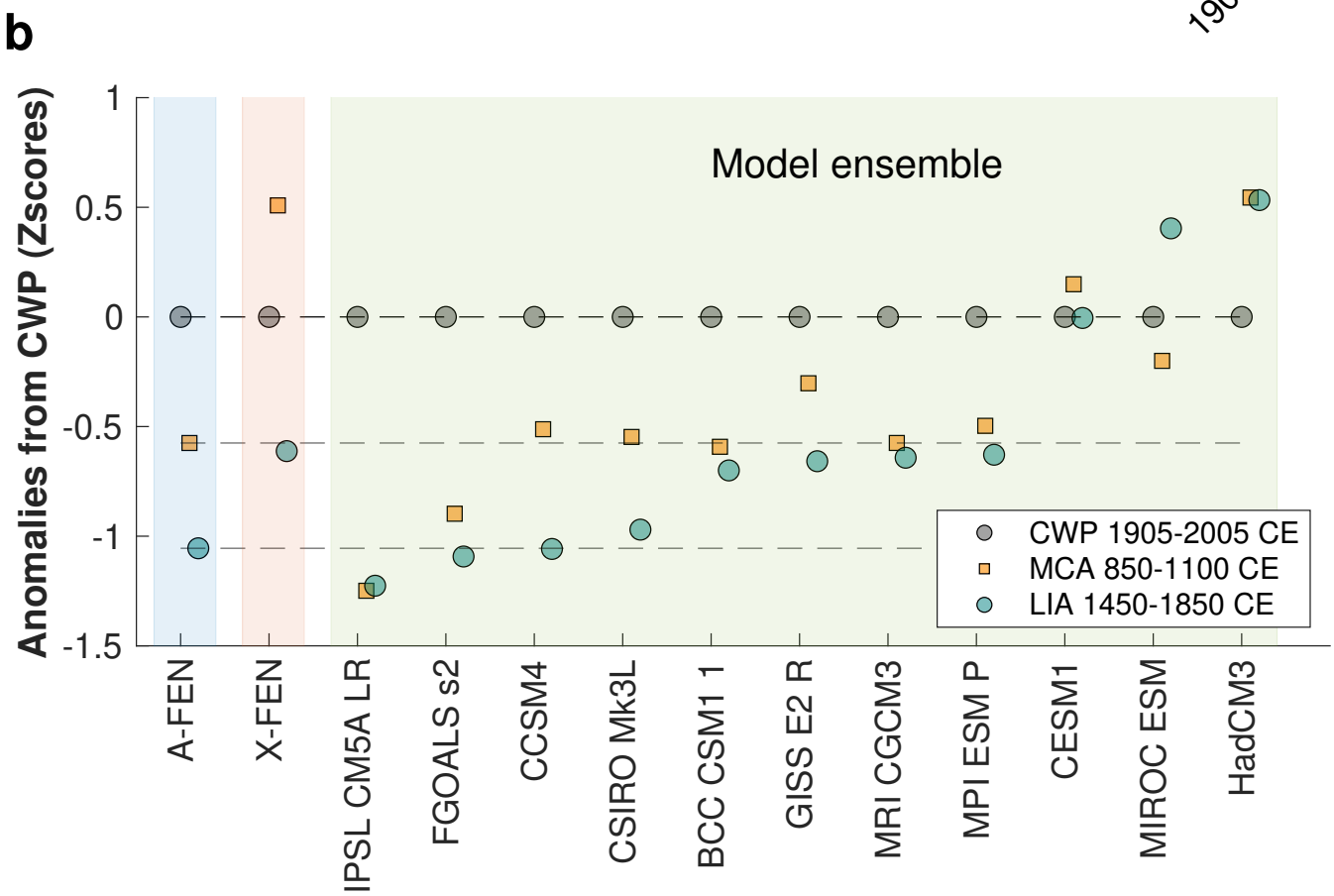
b
Anomalies from CWP (Zscores)
1
0.5
0
-0.5
-1
-1.5
Model ensemble
CWP 1905-2005 CE
MCA 850-1100 CE
LIA 1450-1850 CE
A-FEN
X-FEN
IPSL CM5A LR
FGOALS s2
CCSM4
CSIRO Mk3L
BCC CSM1 1
GISS E2 R
MRI CGCM3
MPI ESM P
CESM1
MIROC ESM
HadCM3

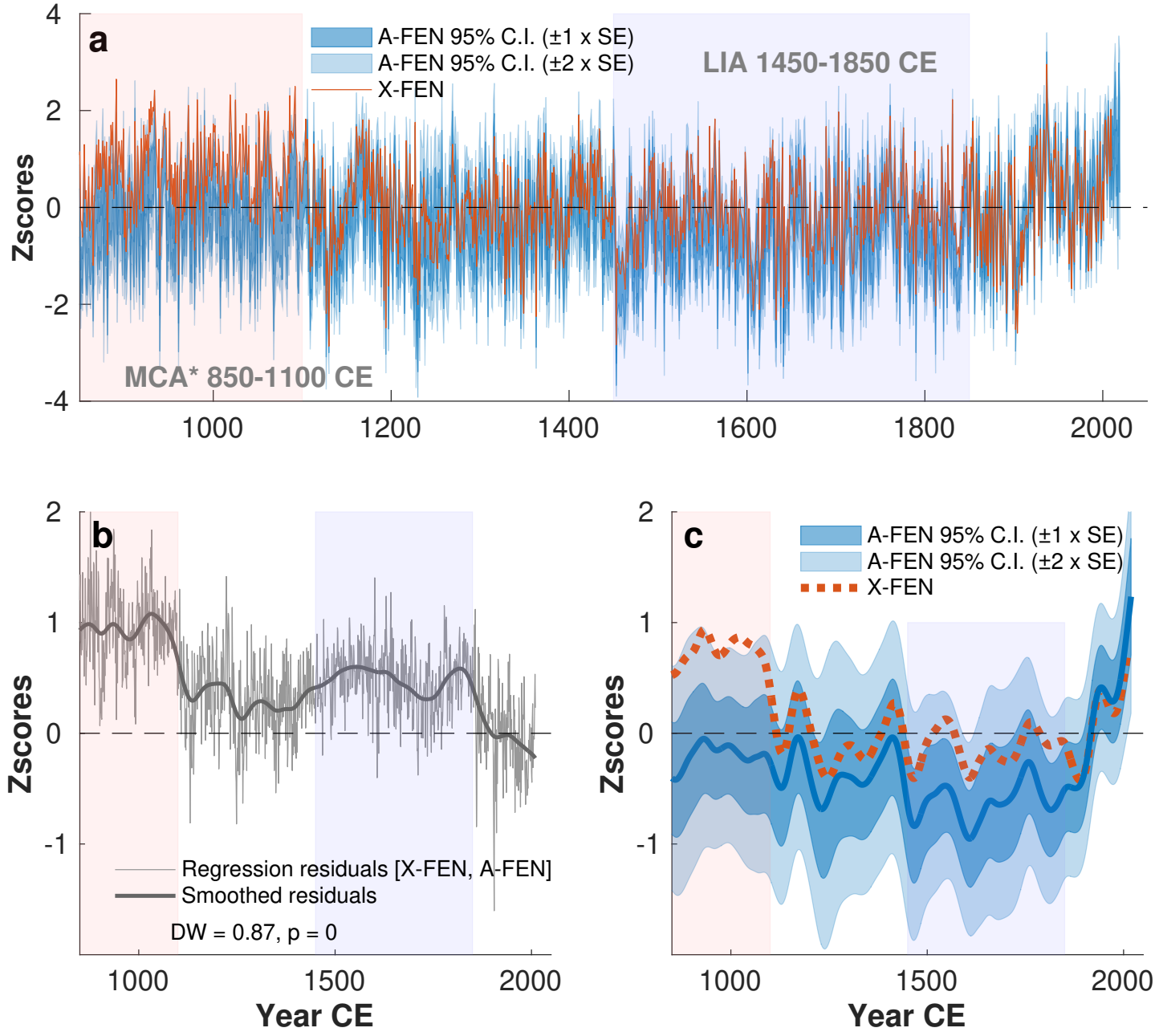
a
A-FEN 95% C.I. (±1 x SE)
A-FEN 95% C.I. (±2 x SE)
X-FEN
LIA 1450-1850 CE
MCA* 850-1100 CE
Zscores
4
2
0
-2
-4
1000
1200
1400
1600
1800
2000
b
Regression residuals [X-FEN, A-FEN]
Smoothed residuals
DW = 0.87, p = 0
Zscores
2
1
0
-1
1000
1500
2000
Year CE
c
A-FEN 95% C.I. (±1 x SE)
A-FEN 95% C.I. (±2 x SE)
X-FEN
Zscores
2
1
0
-1
1000
1500
2000
Year CE